Edge State, Localization Length, and Critical Exponent from Survival Probability in Topological Waveguides

Li-Cheng Wang,[1] Yang Chen,[2,3,4] Ming Gong,[2,3,4] Feng Yu,[1] Qi-Dai Chen,[1] Zhen-Nan Tian,[1,*] Xi-Feng Ren,[2,3,4,†] and Hong-Bo Sun[1,5,‡]

[1]*State Key Laboratory of Integrated Optoelectronics, College of Electronic Science and Engineering, Jilin University, Changchun 130012, China*

[2]*CAS Key Laboratory of Quantum Information, University of Science and Technology of China, Hefei 230026, China*

[3]*CAS Center for Excellence in Quantum Information and Quantum Physics, University of Science and Technology of China, Hefei 230026, China*

[4]*Hefei National Laboratory, University of Science and Technology of China, Hefei 230088, China*

[5]*State Key Laboratory of Precision Measurement Technology and Instruments, Department of Precision Instrument, Tsinghua University, Haidian, Beijing 100084, China*

(Received 30 May 2022; revised 5 August 2022; accepted 20 September 2022; published 18 October 2022)

Edge states in topological phase transitions have been observed in various platforms. To date, verification of the edge states and the associated topological invariant are mostly studied, and yet a quantitative measurement of topological phase transitions is still lacking. Here, we show the direct measurement of edge states and their localization lengths from survival probability. We employ photonic waveguide arrays to demonstrate the topological phase transitions based on the Su-Schrieffer-Heeger model. By measuring the survival probability at the lattice boundary, we show that in the long-time limit, the survival probability is $P = (1 - e^{-2/\xi_{\rm loc}})^2$, where $\xi_{\rm loc}$ is the localization length. This length derived from the survival probability is compared with the distance from the transition point, yielding a critical exponent of $\nu = 0.94 \pm 0.04$ at the phase boundary. Our experiment provides an alternative route to characterizing topological phase transitions and extracting their key physical quantities.

DOI: 10.1103/PhysRevLett.129.173601

Photonic topological insulators [1–4], in which the edge states are robust against perturbations and disorders, have been widely explored in experiments [5–14]. Among them, one of the simplest topological models in one dimension is the Su-Schrieffer-Heeger (SSH) model [15,16]; it can be described by the Dirac equation in the continuous limit. It has been studied in various systems, including topological edge states in optical waveguides [17–22], cold atoms [23–25], quantum dot arrays [26–28], electrical circuits [29–31], and systems with interacting particles [32–35]. However, the literature usually focused on the verification of the existence of edge states predicted by the bulk-boundary correspondence; yet, a full characterization of the localized edge states and their related dynamics as well as a quantitative study of topological phase transitions remain to be experimentally explored.

In the study of topological phases, critical exponents in the vicinity of the transition points are proposed to characterize the universality classes of topological phase transitions [36–38]. For a topological system, the correlation lengths should coincide with their edge-state localization lengths, which have not yet been experimentally confirmed. Here, we fabricate photonic waveguide arrays using a femtosecond laser direct writing technique [39–42] to realize the SSH model with a chain length of $M = 50$ or $M = 51$. We extract their localization length and critical exponent from the measured survival probability in these structures. The major findings are as follows: (I) We demonstrate two distinct long-time propagation dynamics. In topologically trivial phases, the wave packet propagates throughout the space; whereas in topological phases, it remains at the boundary. (II) The survival probability is a unique function of the localization length $\xi_{\rm loc}$ from which the localization length can be extracted directly. (III) At the phase boundary, we extract $\xi_{\rm loc} \sim 1/\epsilon_g^\nu \propto |d_j - d_2|^{-\nu}$ with critical exponent $\nu = 0.94 \pm 0.04$ and energy gap ϵ_g. The relative waveguide separation $|d_1 - d_2|$ corresponds to the distance from the transition point ($d_1 = d_2$). With these results, we can determine the phase diagram and the associated critical boundary from the survival probability. This new method provides an alternative approach to characterizing topological phase transitions and extracting their key physical quantities.

Model and topological edge states.—Our system contains a SSH chain described by [43,44]

$$H = \sum_{j=1}^{N} (t_1 a_j^\dagger b_j + \text{H.c.}) + \sum_{j=1}^{N-1(N)} (t_2 b_j^\dagger a_{j+1} + \text{H.c.}), \quad (1)$$

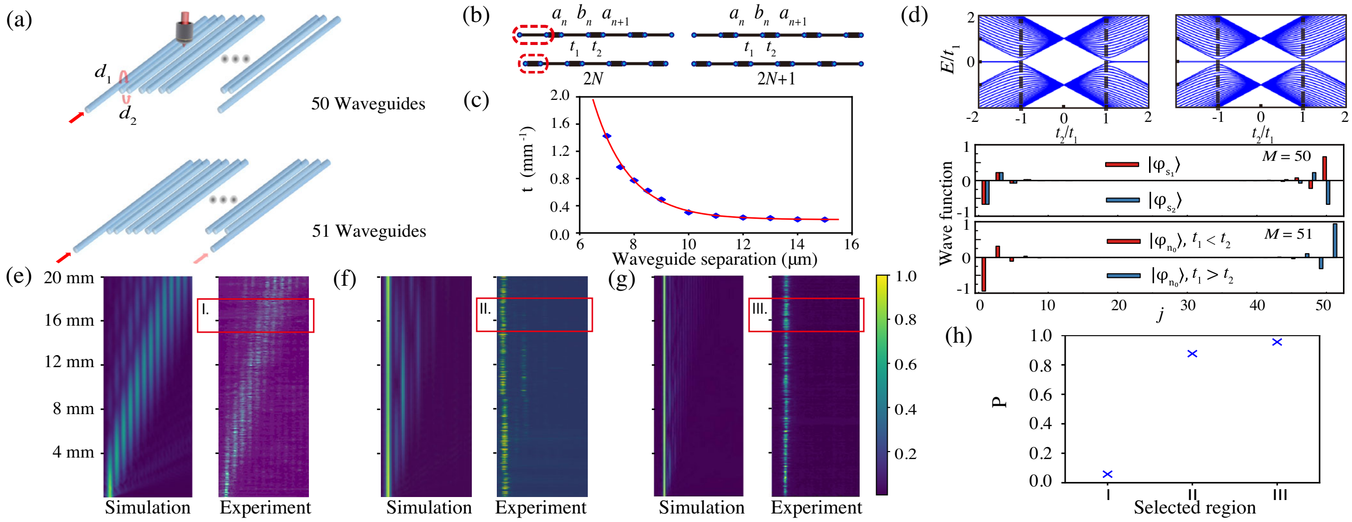

FIG. 1. (a) Experimental study of propagation dynamics with a single excitation. (b) Scheme of even-indexed (left) and odd-indexed (right) SSH chains. Each unit cell (red dashed lines) consists of two sublattices with equal sublattice potential, labeled a and b. Intra- and intercell couplings are t_1 and t_2, respectively. (c) Relation between coupling constant and waveguide separation of two evanescently coupled waveguides. (d) Energy spectra of even-indexed (top left, $M = 50$) and odd-indexed (top right, $M = 51$) chains; $|\phi_{s_i}\rangle$, $i = 1, 2$ (middle): wave functions of two hybridized edge states ($t_1/t_2 = 1/3$, $M = 50$); $|\phi_{n_0}\rangle$ (bottom): wave function of left (red bar, $t_1/t_2 = 1/3$) or right edge state (blue bar, $t_1/t_2 = 3$) for $M = 51$. (e)–(g) Numerical (left) and experimental (right) results of intensity distribution along propagation direction. (e) Ballistic transport of light when $d_1 = d_2 = 11$ μm. (f) Localization of light when $d_1/d_2 = 13/10$ μm (topological). (g) Stronger localization when $d_1/d_2 = 13/8$ μm. (h) Measured mean survival probability at selected regions (red rectangles) in Figs. 1(e)–1(g).

where $a_j^\dagger$ ($b_j^\dagger$) and a_j (b_j) are the creation and annihilation operators of particles at the a (b) sublattices of the jth unit cell [see Fig. 1(b)], respectively. The dimerized waveguide arrays with alternating intra- or intercell waveguide separations are fabricated using the femtosecond laser direct writing technique, which has been validated as a promising tool for quantum simulations in photonic platforms [5,45–51]. With a beam shaping method realized by a spatial light modulator [40,52–54], we obtain circular waveguides with radii of $r = 3.5$ μm, and the waveguide separation ranges from 8 to 13 μm, with a modified dielectric constant of about $\delta n = 1.5 \times 10^{-3}$, following the theoretical investigation in Ref. [55]. The intra- and intercell hopping amplitudes are t_1 and t_2, which are unique functions of the separations d_1 and d_2, respectively. These couplings decay exponentially with the increasing of the separations d_i [shown in Fig. 1(c)] [56], and the next-nearest-neighboring couplings can be neglected. This model is topologically nontrivial with a winding number of $w = 1$ for $|t_1| < |t_2|$ but topologically trivial with $w = 0$ for $|t_1| > |t_2|$. This can be extracted with eigenvalues in the momentum space: $\varepsilon_\pm(k) = \pm\sqrt{t_1^2 + t_2^2 + 2t_1t_2\cos[k(d_1 + d_2)]}$, and the phase transition is characterized by the winding of $t_1 + t_2 e^{ik(d_1+d_2)}$ in the complex plane. Thus, the energy gap of $\varepsilon_g = 2\delta t$, where $\delta t = t_2 - t_1$, leads to the formation of the edge states at the interface of two topologically distinct domains [43].

We consider two kinds of structures with $M = 50$ and $M = 51$, as shown in Fig. 1(a). A continuous-wave laser is coupled into the leftmost or rightmost waveguide. The wavelength is fixed at 808 nm to ensure the single-mode state of the optical waveguide, whereas the variation of the excitation light wavelength changes the coupling coefficient and the edge band structure, which further affects the propagation dynamics [18,57]. We obtain the intensity distribution from the surface scattered light of the waveguide arrays at the top of the sample, which ensures observation of localization of the edge states and wave propagation dynamics directly [58–60]. The eigenstates and eigenvalues of the above model in a finite chain are

$$|\phi_n\rangle = \sum_i \phi_{ni}|i\rangle$$

and ε_n, respectively, where ϕ_{ni} is the nth eigenstate amplitude in the ith site. The energy spectrum and edge-state wave function of the Hamiltonian with even- (odd-) indexed lattice sites are shown in Fig. 1(d), in which the energy of the states corresponds to the propagation constant of the optical modes [57]. There are two near-zero-energy states when the system is topologically nontrivial for the even-indexed lattice sites, whereas a zero-energy state always exists for the odd-indexed lattice sites (localized either on the left or the right ends due to the dimerization). For an even-indexed chain, the two near-zero-energy eigenstates are hybridized states, which are superposition states that are exponentially localized at the left and right ends of the chain. The energy of the hybridized states is exponentially small in the system size according to $\delta E \sim e^{-M/\xi}$ [44], where M is the chain length and ξ is the localization length. Due to the small energy splitting between the two hybridized states, the propagation distance required for the power to be exchanged between the two ends is quite long. Therefore, the localization length of the system can be obtained by measuring the survival probability at one end, which will be discussed later. In this model, $\xi = 1/\ln(|t_2|/|t_1|)$. The left and right edge-state wave functions can be expressed as

$$|L\rangle = \sum_{j=1}^{N} \alpha_j |j, a\rangle$$

and

$$|R\rangle = \sum_{j=1}^{N} \beta_j |j, b\rangle,$$

where $|\alpha_j| = |\alpha_1| e^{-(j-1)/\xi}$ and $|\beta_j| = |\beta_N| e^{-(N-j)/\xi}$ denote the amplitudes in these a and b sublattices, respectively [44,61]. In the vicinity of the phase boundary, the localization length is governed by $\xi = 1/\varepsilon_g^{\nu}$ [37], where ν is the critical exponent ($\nu = 1$ in theory) and ε_g is the gap width.

Propagation dynamics.—Because the contribution of the bulk states at the localized lattice sites is negligible, the edge states could be experimentally observed by applying a single excitation at the boundary of the lattice and measuring the survival probability of these states remaining at the boundary at the long-time limit [32,62–64]. For those topological systems with multiple edge states or higher topological invariants, the initial excitations may need to be tailored accordingly [57,65–67], and the survival probability may need to be defined at all the localized sites due to the energy coupling between these edge states. In the trivial phase, the edge states are absent; thus, the single excitation should couple to all the bulk states, yielding much more complicated behaviors. We consider the case of a single excitation at the boundary of the chain with $|\Psi(0)\rangle = |0\rangle$, and

$$|\Psi(t)\rangle = \sum_{j=0}^{M-1} c_j(t) |j\rangle$$

where $c_j(0) = \delta_{0j}$. The wave dynamics is derived by solving the Schrödinger equation $i\hbar\partial\Psi/\partial t = H\Psi$, where H is given in Eq. (1) under the tight-binding approximation. By assuming that H is time independent, we find

$$c_j(t) = \sum_n e^{-i\varepsilon_n t/\hbar} \phi_{n,0} \phi_{n,j}.$$

This is achieved in our experiments using waveguide arrays with propagation-independent couplings, which are described by the coupled-mode equations [68,69]. Thus, the survival probability at the boundary is given by

$$P = |c_1(t)|^2 = P_0 + P_1(t), \tag{2}$$

$$P_0 = \sum_{n=1}^{M} \phi_{n,0}^4, \qquad P_1(t) = \sum_{i=1}^{M} \sum_{j=i+1}^{M} 2\phi_{i,0}^2 \phi_{j,0}^2 \cos(\varepsilon_i - \varepsilon_j)t. \tag{3}$$

Because H is Hermitian, $|\phi_n\rangle$ is a real vector. The survival probability is decoupled into two different parts, i.e., the time-independent term P_0 and the time-varying term P_1. For the extended modes with nondegenerate eigenvalues, the second term can be neglected in the long-time limit from the cancellation between different modes.

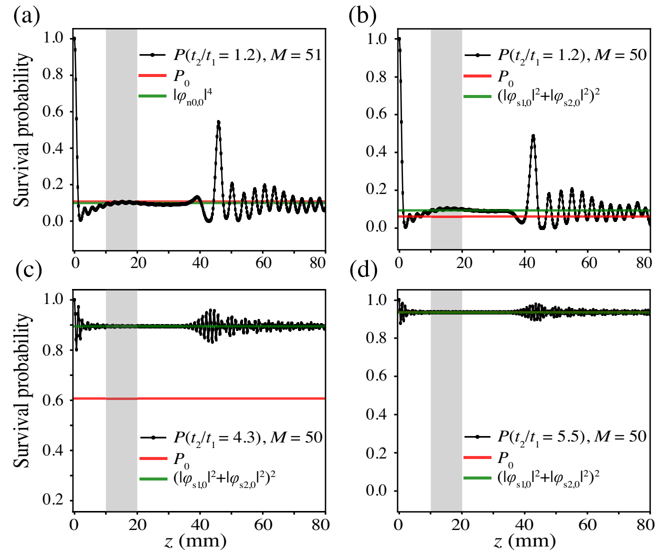

FIG. 2. Survival probability with a single site excitation at the boundary. (a) Time evolution of odd-indexed chain for $t_2/t_1 = 1.2$, and $\bar{P}$ estimated by $|\phi_{n_0,0}|^4$ when the evolution distance is in the range of 10 to 20 mm (shaded region). (b)–(d) Evolutions of even-indexed chain for $t_2/t_1 = \{1.2, 4.3, 5.5\}$; $\bar{P}$ can be estimated by $(|\phi_{s_1,0}|^2 + |\phi_{s_2,0}|^2)^2$.

The numerical simulations of the propagation dynamics are shown in Fig. 2. For the odd-indexed chain in Fig. 2(a), the first term is reduced to $P_0 \sim |\phi_{n_0,0}|^4$, which is dominated by the contribution of the zero-energy state. The oscillating term $P_1(t)$ can be neglected in the interval of about $z \sim 10$ to 20 mm. In the long-time limit, a finite oscillation of $P_1(t)$ can still be found, which is arising from the constructive interference of the extended modes and can be suppressed with the increase of the system size. For the even-indexed chain in Figs. 2(b)–2(d), we have

$$P \sim |\phi_{s_1,0}|^4 + |\phi_{s_2,0}|^4 + 2|\phi_{s_1,0}|^2 |\phi_{s_2,0}|^2 \cos(\Delta\varepsilon t)$$

due to the presence of two near-degenerate edge modes, where the contributions of the two hybridized states in the P_1 term are included; thus, the mean value

$\bar{P} \sim (|\phi_{s_1,0}|^2 + |\phi_{s_2,0}|^2)^2$. We find that in the interval of $z \sim 10$ to 20 mm, the oscillating term is negligible, and we choose the sample length as 20 mm. In the experiments, we use the mean value over a finite interval to extract the survival probability; i.e.,

$$\bar{P}(T) = \frac{1}{\Delta T}\int_T^{T+\Delta T} P(t)dt,$$

with $\Delta T = 3$ mm [see Figs. 1(e)–1(h)]. In that way, we can also reduce some errors caused by background noise and image noise. Meanwhile, the interval should not be too long to involve the unstable region.

Then, we show that the survival probability is a unique function of the localization length ξ of the edge modes. To this end, we first consider the odd-indexed chain with

$$|L_{n_0}\rangle = \mathcal{A}\sum_{j=0}^{N} e^{-j/\xi}|j,a\rangle$$

($\mathcal{A}$ is the normalization constant). We find that $\bar{P} \sim |\alpha_1|^4 = (1 - e^{-2/\xi})^2/(1 - e^{-2N/\xi})^2$. In the long-chain limit, we have

$$P(\xi_{\rm loc}) = (1 - e^{-(2/\xi_{\rm loc})})^2, \tag{4}$$

where $\xi_{\rm loc}$ is the localization length of the edge state. For the even-indexed chain, due to the hybridization of the two edge states $|L\rangle$ and $|R\rangle$, the eigenstates of the two near-degenerate modes are approximated as $|\phi_{s_{1,2}}\rangle = (e^{-i\theta/2}|L\rangle \pm e^{i\theta/2}|R\rangle)/\sqrt{2}$ with $\theta \in [0, 2\pi)$ [44,70]; thus, $\bar{P} \sim (|\phi_{s_1,0}|^2 + |\phi_{s_2,0}|^2)^2 = |\alpha_1|^4$, yielding the same expression in the long-chain limit, and this relation is true with multiple site excitations involving the localized sites. Thus, when $\xi_{\rm loc}$ is large enough ($\xi > 10$), we have $P(\xi_{\rm loc}) \propto \xi_{\rm loc}^{-2}$, which is a general result.

Dimerization-dependent localization.—Next, we fabricate 36 even-indexed and 36 odd-indexed waveguide arrays with different waveguide separations and explore how the localization is influenced by the dimerization (t_2/t_1). We vary the intracell and intercell distances from 8 to 13 μm in steps of 1 μm. For even-indexed chains, the light is injected and the survival probabilities are measured at the left end of the chain [see Fig. 3(a)]. We obtain different degrees of localization of light at the input site when $t_1 < t_2$ (topological bulk band); however, when $t_1 > t_2$ (trivial bulk band), the edge modes are absent, and the light is diffracted into all the extended bulk modes, yielding small survival probabilities. A sharp boundary is clearly shown at $d_1 = d_2$. For the odd-indexed chains, it is worth noting that the lattice with a trivial bulk band hosts an edge state localized at the right end [Fig. 1(d)], and the localization length can be obtained by applying an excitation at the right end, following the same procedure. Thus, the light is injected and measured at the left end of the chain when

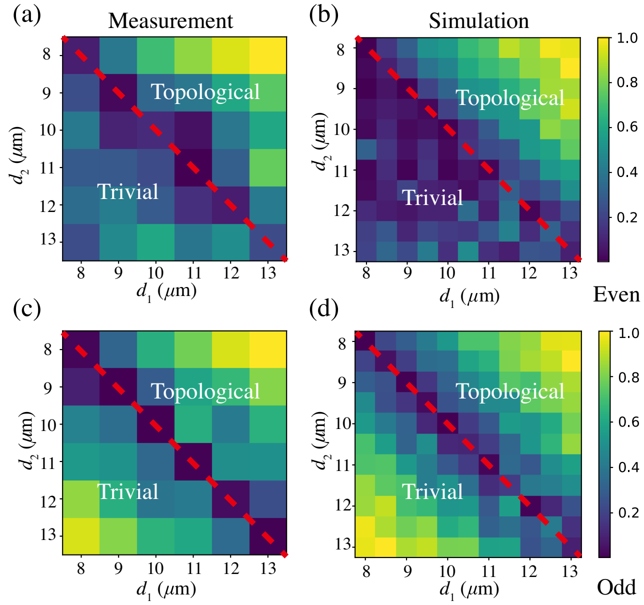

FIG. 3. Left (right): measured (simulated) survival probabilities of the SSH chains. (a)–(b) $M = 50$; (c)–(d) $M = 51$. When $d_1 < d_2$ (trivial bulk band), light diffuses into the bulk of the even-indexed chains, but is localized at the right end of the odd-indexed chains. When $d_1 > d_2$ (topological bulk band), light remains localized at the right end of the chain for both cases. Topological phase transitions are obtained at the transition point $d_1 = d_2$. All survival probabilities are renormalized based on the maximum value.

$t_1 < t_2$ and at the right end when $t_1 > t_2$ [see Fig. 3(c)], in which we observe edge modes at the left and right ends, respectively. As shown in Figs. 3(b) and 3(d), numerical simulations with a step of 0.5 μm are performed based on the beam propagation method [71,72] and agree well with the experimental results. These results demonstrate that the edge modes of the even-indexed and odd-indexed chains exhibit totally different behaviors, which can be clearly distinguished from the measured survival probability. At the phase boundary with $\xi_{\rm loc} \sim M$, we show that the survival probability approaches zero.

Survival probability, localization length, and critical exponent near the phase boundary.—Finally, we investigate the relation between the survival probability and the localization length ($|t_1| < |t_2|$). We fabricate 10 sets of even-indexed and odd-indexed waveguide arrays, with $d_2 = 8$ μm and d_1 ranging from 8.5 to 13 μm. The measured survival probabilities for various configurations are shown in Fig. 4(a). In Fig. 4(b), we show the relation between the survival probability and the localization length derived by $1/\ln(|t_2|/|t_1|)$, which agrees excellently with Eq. (4), both experimentally and numerically. Based on this analytical expression, we use the measured survival probabilities to determine the corresponding localization lengths $\xi_{\rm exp}$ of our sample, and they are compared with the numerical and the analytical results using $\xi_{\rm the} = 1/\ln(|t_2|/|t_1|)$ [Fig. 4(c)], exhibiting excellent agreement.

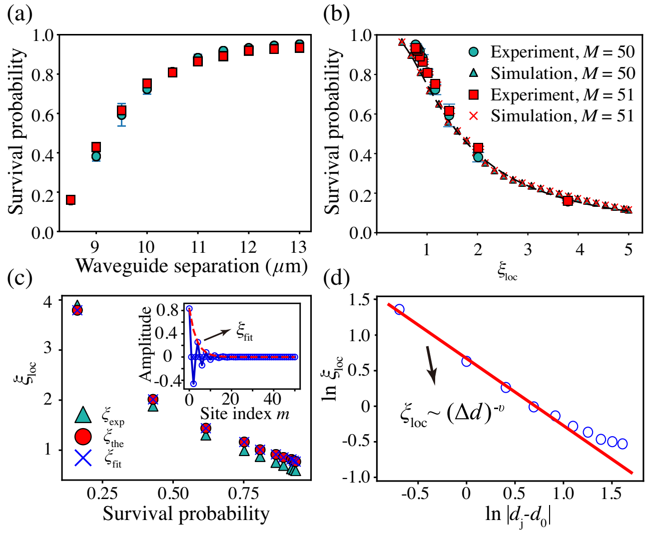

FIG. 4. (a) Measured survival probability P for $M = 50$ and $M = 51$. (b) Numerical and experimental results of P versus $\xi_{\rm loc}$. The black dashed line is plotted using Eq. (4). All error bars denote one standard deviation of the data averaged over three independent measurements. (c) Localization lengths from the measured survival probabilities ($M = 51$) using Eq. (4), which are compared with the analytical results of $\xi_{\rm the} = 1/\ln(|t_2|/|t_1|)$ and the numerical results (see the inset). (d) Critical exponent extracted from $\xi_{\rm loc}$ (by experiment) and the control parameter $\Delta d = |d_j - d_0|$ ($d_0 = 8\ \mu$m), near the phase boundary, yielding $\nu = 0.94 \pm 0.04$.

As shown in Fig. 4(d), with the localization length $\xi_{\rm loc}$ extracted from the measured survival probabilities and the control parameters, in which $\varepsilon_g \propto |d_1 - d_2|$, we have $\xi_{\rm loc} \propto \varepsilon_g^{-\nu} \propto |d_1 - d_2|^{-\nu}$ near the transition point. The fitted critical exponent of $\nu = 0.94$ agrees excellently with our theoretical prediction of $\nu = 1$.

Conclusions.—We experimentally demonstrated the edge state, the localization length, and the critical exponent from the survival probability. We fabricated photonic waveguides with various structures and determined the phase transitions from this approach, which were based on a relation in which the survival probability is a unique function of the localization length. Compared with the conventional end-face imaging, the proposed idea could be applied in the exploration of critical phenomena near the phase transition point in complicated unknown systems [60,73,74], such as topological phase transitions in two-dimensional models with high topological invariants. Although direct imaging of the wave propagation for higher-dimensional models might be a tricky task, we find that the stray light from out-of-focus planes can be effectively suppressed with further improvement of our system using a confocal microscopic system [75].

Furthermore, because the complex refractive index profiles can be introduced in photonic lattices [76–81], we anticipate that our findings will facilitate the study of transport behavior and critical phenomena in non-Hermitian systems. In such lossy systems, more advanced imaging techniques might be required to achieve the desired measurement accuracy. In particular, it would be quite interesting to extend such methods to study the dynamics of local Chern markers near the transition point [82,83], which helps to uncover exotic topological phases.

This research is supported by the National Natural Science Foundation of China (Nos. 61960206003, 61825502, 61827826, 62061160487, and 12204462), the Innovation Program for Quantum Science and Technology (No. 2021ZD0303200), and the Fundamental Research Funds for the Central Universities. This work was partially carried out at the USTC Center for Micro and Nanoscale Research and Fabrication.

L. C. Wang and Y. Chen contributed equally to this work.

*zhennan_tian@jlu.edu.cn
†renxf@ustc.edu.cn
‡hbsun@tsinghua.edu.cn

[1] F. D. M. Haldane and S. Raghu, Possible Realization of Directional Optical Waveguides in Photonic Crystals with Broken Time-Reversal Symmetry, Phys. Rev. Lett. **100**, 013904 (2008).
[2] M. Z. Hasan and C. L. Kane, Colloquium: Topological insulators, Rev. Mod. Phys. **82**, 3045 (2010).
[3] Ling Lu, John D. Joannopoulos, and Marin Soljačić, Topological photonics, Nat. Photonics **8**, 821 (2014).
[4] T. Ozawa, H. M. Price, A. Amo, N. Goldman, M. Hafezi, L. Lu, M. C. Rechtsman, D. Schuster, J. Simon, O. Zilberberg, and I. Carusotto, Topological photonics, Rev. Mod. Phys. **91**, 015006 (2019).
[5] Stefano Longhi, Quantum-optical analogies using photonic structures, Laser Photonics Rev. **3**, 243 (2009).
[6] Zheng Wang, Yidong Chong, John D. Joannopoulos, and Marin Soljačić, Observation of unidirectional backscattering-immune topological electromagnetic states, Nature (London) **461**, 772 (2009).
[7] Mohammad Hafezi, Eugene A. Demler, Mikhail D. Lukin, and Jacob M. Taylor, Robust optical delay lines with topological protection, Nat. Phys. **7**, 907 (2011).
[8] S. Mittal, J. Fan, S. Faez, A. Migdall, J. M. Taylor, and M. Hafezi, Topologically Robust Transport of Photons in a Synthetic Gauge Field, Phys. Rev. Lett. **113**, 087403 (2014).
[9] P. St-Jean, V. Goblot, E. Galopin, A. Lemaitre, T. Ozawa, L. Le Gratiet, I. Sagnes, J. Bloch, and A. Amo, Lasing in topological edge states of a one-dimensional lattice, Nat. Photonics **11**, 651 (2017).
[10] Zhaoju Yang, Eran Lustig, Yaakov Lumer, and Mordechai Segev, Photonic floquet topological insulators in a fractal lattice, Light **9**, 128 (2020).
[11] Avik Dutt, Momchil Minkov, Ian A. D. Williamson, and Shanhui Fan, Higher-order topological insulators in synthetic dimensions, Light **9**, 131 (2020).
[12] Yang Chen, Xin-Tao He, Yu-Jie Cheng, Hao-Yang Qiu, Lan-Tian Feng, Ming Zhang, Dao-Xin Dai, Guang-Can

Guo, Jian-Wen Dong, and Xi-Feng Ren, Topologically Protected Valley-Dependent Quantum Photonic Circuits, Phys. Rev. Lett. **126**, 230503 (2021).
[13] Alexander Cerjan, Mohan Wang, Sheng Huang, Kevin P. Chen, and Mikael C. Rechtsman, Thouless pumping in disordered photonic systems, Light **9**, 178 (2020).
[14] Tianxiang Dai, Yutian Ao, Jueming Bao, Jun Mao, Yulin Chi, Zhaorong Fu, Yilong You, Xiaojiong Chen, Chonghao Zhai, Bo Tang *et al.*, Topologically protected quantum entanglement emitters, Nat. Photonics **16**, 248 (2022).
[15] Roman Jackiw and Cláudio Rebbi, Solitons with fermion number $1/2$, Phys. Rev. D **13**, 3398 (1976).
[16] W. P. Su, J. R. Schrieffer, and A. J. Heeger, Solitons in Polyacetylene, Phys. Rev. Lett. **42**, 1698 (1979).
[17] Natalia Malkova, Ivan Hromada, Xiaosheng Wang, Garnett Bryant, and Zhigang Chen, Observation of optical Shockley-like surface states in photonic superlattices, Opt. Lett. **34**, 1633 (2009).
[18] Andrea Blanco-Redondo, Imanol Andonegui, Matthew J. Collins, Gal Harari, Yaakov Lumer, Mikael C. Rechtsman, Benjamin J. Eggleton, and Mordechai Segev, Topological Optical Waveguiding in Silicon and the Transition Between Topological and Trivial Defect States, Phys. Rev. Lett. **116**, 163901 (2016).
[19] Midya Parto, Steffen Wittek, Hossein Hodaei, Gal Harari, Miguel A. Bandres, Jinhan Ren, Mikael C. Rechtsman, Mordechai Segev, Demetrios N. Christodoulides, and Mercedeh Khajavikhan, Edge-Mode Lasing in 1D Topological Active Arrays, Phys. Rev. Lett. **120**, 113901 (2018).
[20] Yao Wang, Xiao-Ling Pang, Yong-Heng Lu, Jun Gao, Yi-Jun Chang, Lu-Feng Qiao, Zhi-Qiang Jiao, Hao Tang, and Xian-Min Jin, Topological protection of two-photon quantum correlation on a photonic chip, Optica **6**, 955 (2019).
[21] Chenlei Li, Ming Zhang, Hongnan Xu, Ying Tan, Yaocheng Shi, and Daoxin Dai, Subwavelength silicon photonics for on-chip mode-manipulation, PhotoniX **2**, 11 (2021).
[22] Zhi-Qiang Jiao, Stefano Longhi, Xiao-Wei Wang, Jun Gao, Wen-Hao Zhou, Yao Wang, Yu-Xuan Fu, Li Wang, Ruo-Jing Ren, Lu-Feng Qiao, and Xian-Min Jin, Experimentally Detecting Quantized Zak Phases Without Chiral Symmetry in Photonic Lattices, Phys. Rev. Lett. **127**, 147401 (2021).
[23] Marcos Atala, Monika Aidelsburger, Julio T. Barreiro, Dmitry Abanin, Takuya Kitagawa, Eugene Demler, and Immanuel Bloch, Direct measurement of the Zak phase in topological Bloch bands, Nat. Phys. **9**, 795 (2013).
[24] Eric J. Meier, Fangzhao Alex An, and Bryce Gadway, Observation of the topological soliton state in the Su-Schrieffer-Heeger model, Nat. Commun. **7**, 13986 (2016).
[25] Dizhou Xie, Wei Gou, Teng Xiao, Bryce Gadway, and Bo Yan, Topological characterizations of an extended Su-Schrieffer-Heeger model, npj Quantum Inf. **5**, 55 (2019).
[26] Jay D. Sau and S. Das Sarma, Realizing a robust practical Majorana chain in a quantum-dot-superconductor linear array, Nat. Commun. **3**, 964 (2012).
[27] Beatriz Pérez-González, Miguel Bello, Gloria Platero, and Álvaro Gómez-León, Simulation of 1D Topological Phases in Driven Quantum Dot Arrays, Phys. Rev. Lett. **123**, 126401 (2019).
[28] Timo Hyart and Jose L. Lado, Non-Hermitian many-body topological excitations in interacting quantum dots, Phys. Rev. Res. **4**, L012006 (2022).
[29] Stefan Imhof, Christian Berger, Florian Bayer, Johannes Brehm, Laurens W. Molenkamp, Tobias Kiessling, Frank Schindler, Ching Hua Lee, Martin Greiter, Titus Neupert *et al.*, Topolectrical-circuit realization of topological corner modes, Nat. Phys. **14**, 925 (2018).
[30] Nikita A. Olekhno, Egor I. Kretov, Andrei A. Stepanenko, Polina A. Ivanova, Vitaly V. Yaroshenko, Ekaterina M. Puhtina, Dmitry S. Filonov, Barbara Cappello, Ladislau Matekovits, and Maxim A. Gorlach, Topological edge states of interacting photon pairs emulated in a topolectrical circuit, Nat. Commun. **11**, 1436 (2020).
[31] A. Stegmaier, S. Imhof, T. Helbig, T. Hofmann, C. H. Lee, M. Kremer, A. Fritzsche, T. Feichtner, S. Klembt, S. Hofling, I. Boettcher, I. C. Fulga, L. Ma, O. G. Schmidt, M. Greiter, T. Kiessling, A. Szameit, and R. Thomale, Topological Defect Engineering and PT Symmetry in Non-Hermitian Electrical Circuits, Phys. Rev. Lett. **126**, 215302 (2021).
[32] P. Nevado, S. Fernandez-Lorenzo, and D. Porras, Topological Edge States in Periodically Driven Trapped-Ion Chains, Phys. Rev. Lett. **119**, 210401 (2017).
[33] Andrew Hayward, Christian Schweizer, Michael Lohse, Monika Aidelsburger, and Fabian Heidrich-Meisner, Topological charge pumping in the interacting bosonic Rice-Mele model, Phys. Rev. B **98**, 245148 (2018).
[34] Lebing Chen, Jae-Ho Chung, Bin Gao, Tong Chen, Matthew B. Stone, Alexander I. Kolesnikov, Qingzhen Huang, and Pengcheng Dai, Topological Spin Excitations in Honeycomb Ferromagnet CrI_3, Phys. Rev. X **8**, 041028 (2018).
[35] Sylvain de Léséleuc, Vincent Lienhard, Pascal Scholl, Daniel Barredo, Sebastian Weber, Nicolai Lang, Hans Peter Büchler, Thierry Lahaye, and Antoine Browaeys, Observation of a symmetry-protected topological phase of interacting bosons with Rydberg atoms, Science **365**, 775 (2019).
[36] Wei Chen, Markus Legner, Andreas Rüegg, and Manfred Sigrist, Correlation length, universality classes, and scaling laws associated with topological phase transitions, Phys. Rev. B **95**, 075116 (2017).
[37] Alvaro Ferraz, Kumar S. Gupta, Gordon Walter Semenoff, and Pasquale Sodano, *Strongly Coupled Field Theories for Condensed Matter and Quantum Information Theory*, Springer Proceedings in Physics Vol. 239 (Springer, New York, 2020), 10.1007/978-3-030-35473-2.
[38] Mohsin Iqbal and Norbert Schuch, Entanglement Order Parameters and Critical Behavior for Topological Phase Transitions and Beyond, Phys. Rev. X **11**, 041014 (2021).
[39] Rafael R. Gattass and Eric Mazur, Femtosecond laser micromachining in transparent materials, Nat. Photonics **2**, 219 (2008).
[40] Zhen-Ze Li, Lei Wang, Hua Fan, Yan-Hao Yu, Hong-Bo Sun, Saulius Juodkazis, and Qi-Dai Chen, O-FIB: Far-field-induced near-field breakdown for direct nanowriting in an atmospheric environment, Light **9**, 41 (2020).
[41] Jiayu Liu, Zongwei Xu, Ying Song, Hong Wang, Bing Dong, Shaobei Li, Jia Ren, Qiang Li, Mathias Rommel,

Xinhua Gu, Bowen Liu, Minglie Hu, and Fengzhou Fang, Confocal photoluminescence characterization of silicon-vacancy color centers in 4H-SiC fabricated by a femtosecond laser, Nanotechnol. Precis. Eng. **3**, 218 (2020).
[42] Zhuo-Chen Ma, Yong-Lai Zhang, Bing Han, Xin-Yu Hu, Chun-He Li, Qi-Dai Chen, and Hong-Bo Sun, Femtosecond laser programmed artificial musculoskeletal systems, Nat. Commun. **11**, 4536 (2020).
[43] Shun-Qing Shen, *Topological Insulators* (Springer, New York, 2012), Vol. 174.
[44] János K. Asbóth, László Oroszlány, and András Pályi, A short course on topological insulators, Lect. Notes Phys. **919**, 997 (2016).
[45] Alexander Szameit and Stefan Nolte, Discrete optics in femtosecond-laser-written photonic structures, J. Phys. B **43**, 163001 (2010).
[46] Mikael C. Rechtsman, Julia M. Zeuner, Yonatan Plotnik, Yaakov Lumer, Daniel Podolsky, Felix Dreisow, Stefan Nolte, Mordechai Segev, and Alexander Szameit, Photonic Floquet topological insulators, Nature (London) **496**, 196 (2013).
[47] Fulvio Flamini, Lorenzo Magrini, Adil S Rab, Nicolò Spagnolo, Vincenzo D'Ambrosio, Paolo Mataloni, Fabio Sciarrino, Tommaso Zandrini, Andrea Crespi, Roberta Ramponi, and Roberto Osellam, Thermally reconfigurable quantum photonic circuits at telecom wavelength by femtosecond laser micromachining, Light **4**, e354 (2015).
[48] Xiao-Yun Xu, Xiao-Wei Wang, Dan-Yang Chen, C. Morais Smith, and Xian-Min Jin, Quantum transport in fractal networks, Nat. Photonics **15**, 703 (2021).
[49] Giacomo Corrielli, Andrea Crespi, and Roberto Osellame, Femtosecond laser micromachining for integrated quantum photonics, Nanophotonics **10**, 3789 (2021).
[50] Feng Yu, Li-Cheng Wang, Yang Chen, Qi-Dai Chen, Zhen-Nan Tian, Xi-Feng Ren, and Hong-Bo Sun, Polarization independent quantum devices with ultra-low birefringence glass waveguides, J. Lightwave Technol. **39**, 1451 (2021).
[51] Yao Zhao, Yang Chen, Zhi-Shan Hou, Bing Han, Hua Fan, Lin-Han Lin, Xi-Feng Ren, and Hong-Bo Sun, Polarization-dependent Bloch oscillations in optical waveguides, Opt. Lett. **47**, 617 (2022).
[52] L. Huang, P. S. Salter, F. Payne, and M. J. Booth, Aberration correction for direct laser written waveguides in a transverse geometry, Opt. Express **24**, 10565 (2016).
[53] Patrick S. Salter and Martin J. Booth, Adaptive optics in laser processing, Light **8**, 110 (2019).
[54] Ze-Zheng Li, Xiao-Yan Li, Feng Yu, Qi-Dai Chen, Zhen-Nan Tian, and Hong-Bo Sun, Circular cross section waveguides processed by multi-foci-shaped femtosecond pulses, Opt. Lett. **46**, 520 (2021).
[55] Yang Chen, Xiao-Man Chen, Xi-Feng Ren, Ming Gong, and Guang-Can Guo, Tight-binding model in optical waveguides: Design principle and transferability for simulation of complex photonics networks, Phys. Rev. A **104**, 023501 (2021).
[56] Alexander Szameit, Felix Dreisow, Thomas Pertsch, Stefan Nolte, and Andreas Tünnermann, Control of directional evanescent coupling in fs laser written waveguides, Opt. Express **15**, 1579 (2007).
[57] Jiho Noh, Sheng Huang, Kevin P. Chen, and Mikael C. Rechtsman, Observation of Photonic Topological Valley Hall Edge States, Phys. Rev. Lett. **120**, 063902 (2018).
[58] Andrea Crespi, Francesco V. Pepe, Paolo Facchi, Fabio Sciarrino, Paolo Mataloni, Hiromichi Nakazato, Saverio Pascazio, and Roberto Osellame, Experimental Investigation of Quantum Decay at Short, Intermediate, and Long Times via Integrated Photonics, Phys. Rev. Lett. **122**, 130401 (2019).
[59] N. N. Skryabin, S. A. Zhuravitskii, I. V. Dyakonov, M. Yu Saygin, S. S. Straupe, and S. P. Kulik, Universal implementation of arbitrary unitary matrices by femtosecond laser written waveguide lattice, AIP Conf. Proc. **2241**, 020033 (2020).
[60] Lukas J. Maczewsky, Kai Wang, Alexander A. Dovgiy, Andrey E. Miroshnichenko, Alexander Moroz, Max Ehrhardt, Matthias Heinrich, Demetrios N. Christodoulides, Alexander Szameit, and Andrey A. Sukhorukov, Synthesizing multi-dimensional excitation dynamics and localization transition in one-dimensional lattices, Nat. Photonics **14**, 76 (2020).
[61] Zhihao Xu, Rong Zhang, Shu Chen, Libin Fu, and Yunbo Zhang, Fate of zero modes in a finite Su-Schrieffer-Heeger model with PT symmetry, Phys. Rev. A **101**, 013635 (2020).
[62] Petar Jurcevic, Ben P. Lanyon, Philipp Hauke, Cornelius Hempel, Peter Zoller, Rainer Blatt, and Christian F. Roos, Quasiparticle engineering and entanglement propagation in a quantum many-body system, Nature (London) **511**, 202 (2014).
[63] Philip Richerme, Zhe-Xuan Gong, Aaron Lee, Crystal Senko, Jacob Smith, Michael Foss-Feig, Spyridon Michalakis, Alexey V. Gorshkov, and Christopher Monroe, Non-local propagation of correlations in quantum systems with long-range interactions, Nature (London) **511**, 198 (2014).
[64] Zhifeng Zhang, Mohammad Hosain Teimourpour, Jake Arkinstall, Mingsen Pan, Pei Miao, Henning Schomerus, Ramy El-Ganainy, and Liang Feng, Experimental realization of multiple topological edge states in a 1d photonic lattice, Laser Photonics Rev. **13**, 1800202 (2019).
[65] L. Jin, Topological phases and edge states in a non-hermitian trimerized optical lattice, Phys. Rev. A **96**, 032103 (2017).
[66] Mengyao Li, Dmitry Zhirihin, Maxim Gorlach, Xiang Ni, Dmitry Filonov, Alexey Slobozhanyuk, Andrea Alù, and Alexander B. Khanikaev, Higher-order topological states in photonic kagome crystals with long-range interactions, Nat. Photonics **14**, 89 (2020).
[67] Y. V. Kartashov, A. A. Arkhipova, S. A. Zhuravitskii, N. N. Skryabin, I. V. Dyakonov, A. A. Kalinkin, S. P. Kulik, V. O. Kompanets, S. V. Chekalin, L. Torner, and V. N. Zadkov, Observation of Edge Solitons in Topological Trimer Arrays, Phys. Rev. Lett. **128**, 093901 (2022).
[68] Demetrios N. Christodoulides, Falk Lederer, and Yaron Silberberg, Discretizing light behaviour in linear and nonlinear waveguide lattices, Nature (London) **424**, 817 (2003).
[69] Yoav Lahini, Assaf Avidan, Francesca Pozzi, Marc Sorel, Roberto Morandotti, Demetrios N. Christodoulides, and Yaron Silberberg, Anderson Localization and Nonlinearity in One-Dimensional Disordered Photonic Lattices, Phys. Rev. Lett. **100**, 013906 (2008).

[70] Bo-Hung Chen and Dah-Wei Chiou, An elementary rigorous proof of bulk-boundary correspondence in the generalized Su-Schrieffer-Heeger model, Phys. Lett. A **384**, 126168 (2020).

[71] Clifford R. Pollock and Michal Lipson, *Integrated Photonics* (Springer, New York, 2003), Vol. 20, 10.1007/978-1-4757-5522-0

[72] Ginés Lifante Pedrola, *Beam Propagation Method for Design of Optical Waveguide Devices* (Wiley, New York, 2015), 10.1002/9781119083405.

[73] K. Sengupta, Stephen Powell, and Subir Sachdev, Quench dynamics across quantum critical points, Phys. Rev. A **69**, 053616 (2004).

[74] Atanu Rajak and Amit Dutta, Survival probability of an edge majorana in a one-dimensional p-wave superconducting chain under sudden quenching of parameters, Phys. Rev. E **89**, 042125 (2014).

[75] James Jonkman, Claire M. Brown, Graham D. Wright, Kurt I. Anderson, and Alison J. North, Tutorial: Guidance for quantitative confocal microscopy, Nat. Protoc. **15**, 1585 (2020).

[76] T. Eichelkraut, R. Heilmann, S. Weimann, Simon Stützer, Felix Dreisow, Demetrios N. Christodoulides, Stefan Nolte, and Alexander Szameit, Mobility transition from ballistic to diffusive transport in non-hermitian lattices, Nat. Commun. **4**, 2533 (2013).

[77] Feng Yu, Xu-Lin Zhang, Zhen-Nan Tian, Qi-Dai Chen, and Hong-Bo Sun, General Rules Governing the Dynamical Encircling of an Arbitrary Number of Exceptional Points, Phys. Rev. Lett. **127**, 253901 (2021).

[78] Sebabrata Mukherjee and Mikael C. Rechtsman, Observation of Unidirectional Solitonlike Edge States in Nonlinear Floquet Topological Insulators, Phys. Rev. X **11**, 041057 (2021).

[79] Marco S. Kirsch, Yiqi Zhang, Mark Kremer, Lukas J. Maczewsky, Sergey K. Ivanov, Yaroslav V. Kartashov, Lluis Torner, Dieter Bauer, Alexander Szameit, and Matthias Heinrich, Nonlinear second-order photonic topological insulators, Nat. Phys. **17**, 995 (2021).

[80] Marius Jürgensen, Sebabrata Mukherjee, and Mikael C. Rechtsman, Quantized nonlinear thouless pumping, Nature (London) **596**, 63 (2021).

[81] Shiqi Xia, Dimitrios Kaltsas, Daohong Song, Ioannis Komis, Jingjun Xu, Alexander Szameit, Hrvoje Buljan, Konstantinos G. Makris, and Zhigang Chen, Nonlinear tuning of PT symmetry and non-Hermitian topological states, Science **372**, 72 (2021).

[82] Marcello Davide Caio, Gunnar Möller, Nigel R. Cooper, and M. J. Bhaseen, Topological marker currents in Chern insulators, Nat. Phys. **15**, 257 (2019).

[83] Daniel Leykam and Daria A. Smirnova, Probing bulk topological invariants using leaky photonic lattices, Nat. Phys. **17**, 632 (2021).